Journal of Energy Chemistry xxx (xxxx) xxx

Contents lists available at ScienceDirect

Journal of Energy Chemistry

journal homepage: www.elsevier.com/locate/jechem

http://www.journals.elsevier.com/journal-of-energy-chemistry/

Communication

Capacitive charge storage enables an ultrahigh cathode capacity in aluminum-graphene battery

Q1 Hanyan Xu[a], Hao Chen[a,*], Haiwen Lai[b], Zheng Li[a], Xiaozhong Dong[a], Shengying Cai[a], Xingyuan Chu[a], Chao Gao[a,*]

[a] MOE Key Laboratory of Macromolecular Synthesis and Functionalization, Department of Polymer Science and Engineering, Key Laboratory of Adsorption and Separation Materials and Technologies of Zhejiang Province, Zhejiang University, 38 Zheda Road, Hangzhou 310027, Zhejiang, China
[b] Hangzhou Gaoxi Technology Co., Ltd., Liangzhu, Hangzhou 310000, Zhejiang, China

ARTICLE INFO

Article history:
Received 7 August 2019
Revised 24 September 2019
Accepted 26 September 2019
Available online xxx

Keywords:
Al-graphene battery
Intercalated graphene
Capacitive charge storage
Increasing capacity
Exfoliation

ABSTRACT

Aluminum-graphene battery is promising for its abundant raw materials, high power density, ultralong cycle life and superior safety. However, the development of aluminum-graphene battery is currently restricted by its insufficient cathode capacity, calling for a newly developed working mechanism. In addition, an irregular constant increase of the cathode capacity was always observed during cycling, but cannot be explained based on the current understanding. Here, we observed an increase of specific capacity by 60% with stable Coulombic efficiency of 98% during 7000 cycles life of Al-graphene batteries employing $AlCl_3/ET_3NHCl$ electrolyte. We demonstrated this growing cathode capacity is attributed to an increasing contribution of capacitive charge storage during cycling, because a gradually enlarged surface area as capacitive active sites is enabled by the exfoliation of graphitic cathode during the periodic intercalation process. Moreover, the graphene cathode was exfoliated more significantly in $AlCl_3/ET_3NHCl$ than 1-ethyl-3-methylimidazolium chloride-based electrolyte, which results from the heavier stress on the graphene layers caused by the larger intercalants in $AlCl_3/ET_3NHCl$. The common intercalation of cations with $AlCl_4^-$ clusters was therefore supposed to occur during charging. This new proposed mechanism can offer the new thought for future design on high-capacity cathode of Al-ion battery.

© 2019 Published by Elsevier B.V. and Science Press on behalf of Science Press and Dalian Institute of Chemical Physics, Chinese Academy of Sciences

Aluminum-ion battery is a very promising energy storage system owing to its distinct properties of abundance of anode materials and superior safety [1–4]. Graphene is one of the most desirable cathode materials due to its ultrafast charging ability and stable long cycle life [5–10], and the best Al-graphene (Al-G) battery prototype currently approached an energy density of 66 Wh kg^{-1}, an ultrahigh power density of 175 kW kg^{-1}, and an ultralong stable cycle life up to 250,000 cycles [7]. These figures make Al-G battery a competitive alternative to the commercial lead-acid (40 Wh kg^{-1}, 180 W kg^{-1}) and nickel-based battery (50–80 Wh kg^{-1}, 50–1000 W kg^{-1}) [2,11], and show great promise for electric vehicles and grid-scale energy storage applications. However, its current energy density is far less satisfying in contrast with that of commercial Li-ion technology (150–200 Wh kg^{-1}) because of its insufficient cathodic capacity of 120 mAh g^{-1} based on the insertion mechanism of monovalent anions ($AlCl_4^-$) into graphene [12–16]. Hence, the improvement of the cathode capacity is of great importance for future Al-G battery technology, calling for a new understanding and design on graphene-based cathode. In addition, the general phenomenon of irregular constant growth in cathode capacity was commonly observed but hardly explained with the current intercalation-based mechanism (23% growth in graphene cathode capacity after 10,000 cycles [6], and 17% increase in graphitic cathode capacity after 4000 cycles [17]). These require new understandings on the working mechanism of graphene-based cathode of Al-ion battery.

Here, we observed the Al-G battery assembled with $AlCl_3/ET_3NHCl$ electrolyte exhibited a growing high capacity by 60% (from 94 to 150 mAh g^{-1}) yet stable Coulombic efficiency (CE) of roughly 98% over 7000 cycles. We demonstrated this gradually growing cathode capacity results from an increased capacitive charge storage, as the concomitant exfoliation of graphene cathode to achieve a larger surface area during the regular intercalation process. Additionally, the cathode can have a larger surface area in $AlCl_3/ET_3NHCl$ than 1-ethyl-3-methylimidazolium chloride (EMIC)-based electrolyte after the same cycles in the two electrolytes, which indicates more significant exfoliation in $AlCl_3/ET_3NHCl$. This

* Corresponding authors.
E-mail addresses: haochen9@stanford.edu (H. Chen), chaogao@zju.edu.cn (C. Gao).

https://doi.org/10.1016/j.jechem.2019.09.025
2095-4956/© 2019 Published by Elsevier B.V. and Science Press on behalf of Science Press and Dalian Institute of Chemical Physics, Chinese Academy of Sciences

Please cite this article as: H. Xu, H. Chen and H. Lai et al., Capacitive charge storage enables an ultrahigh cathode capacity in aluminum-graphene battery, Journal of Energy Chemistry, https://doi.org/10.1016/j.jechem.2019.09.025

UNCORRECTED PROOF

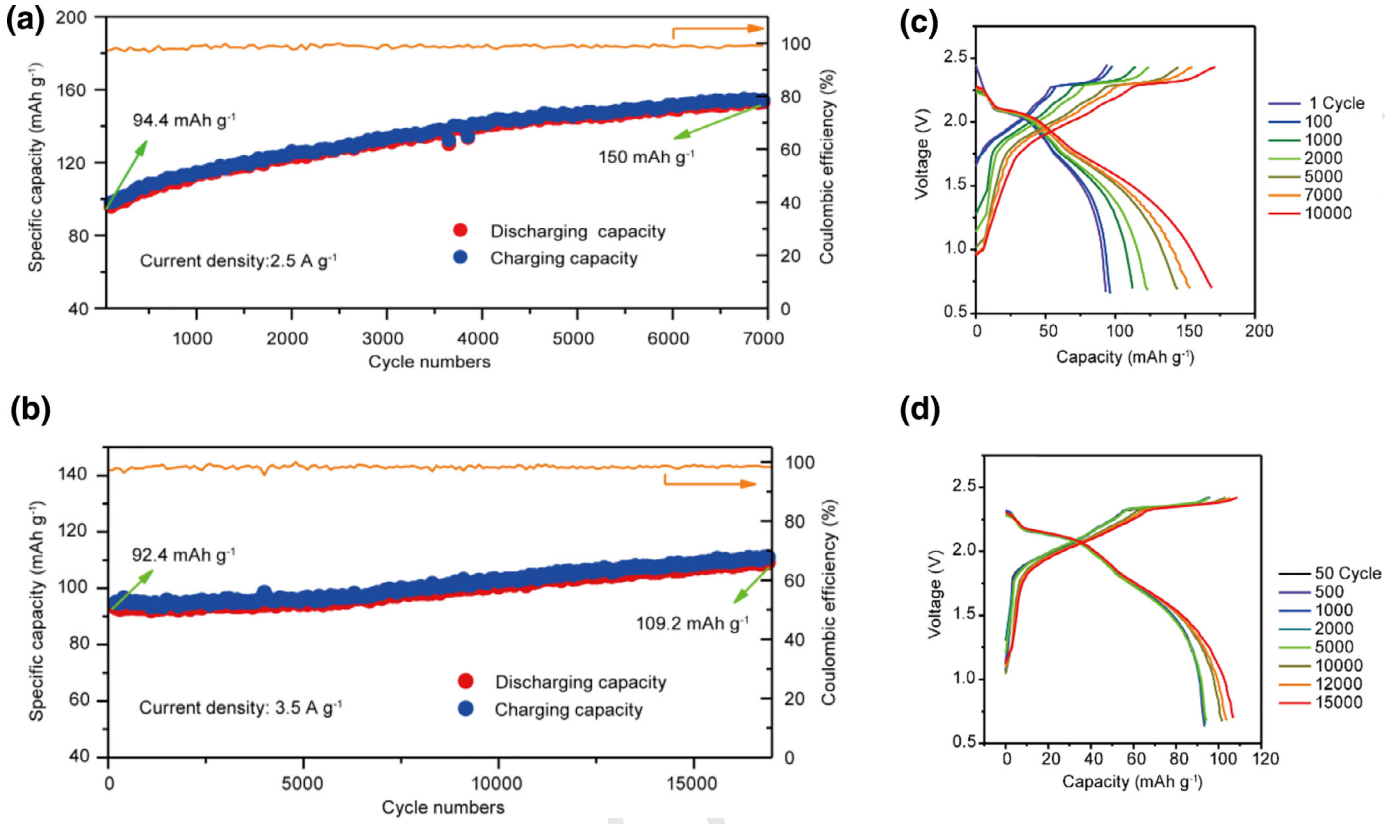


Fig. 1. Galvanostatic cycling of (a) a battery fabricated with Ni current collector, graphene fabric cathode and Et-1.5 electrolyte over 30,000 cycles (current density at 2.5 A g^{-1} and 2.54 V/0.7 V upper/lower cut-off voltage) and (b) a battery assembled with graphene fabric cathode and Emi-1.5 over 20,000 cycles (current density at 3.5 A g^{-1} and 2.49 V/0.7 V upper/lower cut-off voltage). (c) and (d) are their typical galvanostatic curves at different cycles.

serious exfoliation in $AlCl_3/ET_3NHCl$ is because its larger intercalants make the intercalated graphene layers suffer much heavier stress, which confirms that there should have other electrolyte ions intercalated except the believed $AlCl_4^-$ anions during charging. The co-intercalation of ET_3NH^+ with $AlCl_4^-$ clusters is therefore supposed to occur at the low intercalation voltage, and the larger size of ET_3NH^+ than EMI^+ can lead a more serious stripping to the graphene layers. This new understanding on cathodic mechanism gives a new insight on how to improve the cathode capacity of Al-ion battery.

The GF was prepared according to the previous reports of Gao's group [7]. The non-woven graphene fabrics were fabricated through continuous wet-spinning of graphene oxide (GO) fibres and wet-fusing assembly into fabrics. All applied graphene cathodes were processed with high-temperature (3000 °C) annealing [18].

The electrolyte preparation was accorded with the previous work of Dai's and Gao's group [2,19,20].

The Al-G coin cell was fabricated with graphene cathode, aluminum (Al) foil anode, current collector of nickel (Ni) foam or titanium (Ta) foil for cathode, glass fibre paper (Whatman 934-AH, thickness of 435 μm) as separator and 160 μL electrolyte. The coin cell for testing capacitance was fabricated with those cycled graphene cathodes which have been rinsed by super dry CH_2Cl_2 and thoroughly dried, current collector of carbon paper, glass fibre paper as separator and 160 μL electrolyte of $EMIBF_4$ ionic liquid. The coin cells were dismantled by a hydraulic battery remover (HeFei KeJing, China). The re-assembled strategy for replacing the cycled liquid electrolyte with the fresh one was done by firstly immersing the cycled cathode into the fresh electrolyte for over 20 min to minimize the effects from the cycled electrolyte, then removing the used membranes and finally, adding the fresh membranes and liquid electrolyte. The strategy for substituting cycled cathode with fresh one is much easier, cleaning the used cathode on the current collector and then adding a fresh one on it.

Cyclic voltammogram (CV) and electrochemical impedance spectroscopy (EIS) were performed on a Metrohm Multi Autolab. The galvanostatic cycling was performed on a Land BT2000 Battery Test System (Wuhan, China).

In-situ Raman spectra were obtained from an inVia-Reflex micro-Raman spectroscopy system. The morphologies of the electrodes were investigated by scanning electron microscope (SEM) (Hitachi S-3000 N). Powder in-situ X-ray diffraction (XRD) results were examined through a Rigaku Ultima IV X-ray diffractometer with Cu $K\alpha 1$ radiation (1.5406 Å) in the scan range of 18°–35° at a scan rate of 5° min^{-1}. The intercalant gallery height (d_i) is calculated by Eq. (1) where l is the index of (00l) oriented in the stacking direction and d_{obs} is the observed value of the spacing between two adjacent planes [2,21]. X-ray photoelectron spectroscopy (XPS) analysis was through AXIS SUPRA Angular resolution X-ray photoelectron spectrometer. Raman spectroscopy for the chloroaluminate electrolytes was collected from an Au-coated Si chip [2,22].

$$I_c = d_i + 3.35\ \text{Å} \times (n-1) = \Delta d + 3.35\ \text{Å} \times n = l \times d_{obs} \quad (1)$$

We firstly assembled Al-G batteries with Ni current collector, graphene fabric cathode and $EMIC/AlCl_3$ electrolyte at molar ratio 1.3 (r_{AlCl3}=1.3, named Emi-1.3) which showed a cathode capacity of 95 mAh g^{-1} and 20,000 cycles life at current density of 4 A g^{-1} (Fig. S1). This performance is normal, and the capacity is stable with cycles. However, when $ET_3NHCl/AlCl_3$ electrolyte (r_{AlCl3}=1.5, Et-1.5) substituted for Emi-1.3, the capacity of this battery witnessed a steep increase by 60% within 7000 cycles (from 94 to150 mAh g^{-1}, Fig. 1a). While there was a rise by 20% to

UNCORRECTED

Please cite this article as: H. Xu, H. Chen and H. Lai et al., Capacitive charge storage enables an ultrahigh cathode capacity in aluminum-graphene battery, Journal of Energy Chemistry, https://doi.org/10.1016/j.jechem.2019.09.025

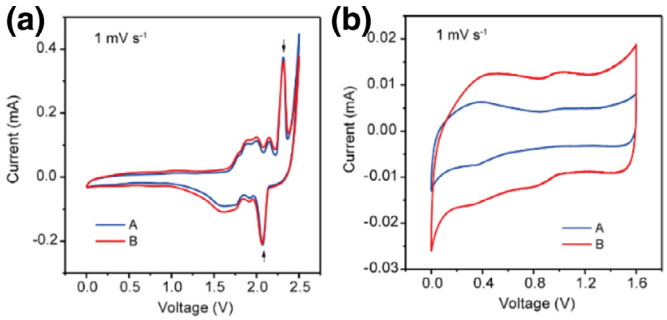


Fig. 2. Cyclic voltammogram (CV) curves of the Al-G battery using Ta current collector and Et-1.5 at a normal status with a discharging capacity of roughly 120 mAh g^{-1} and a CE of 98% (named "A" in the two pictures) and at an abnormal status with a discharging capacity of 170 mAh g^{-1} and a CE of 98% (named "B"), in a scan voltage range of (a) 0–2.5 V and (b) 0–1.6 V.

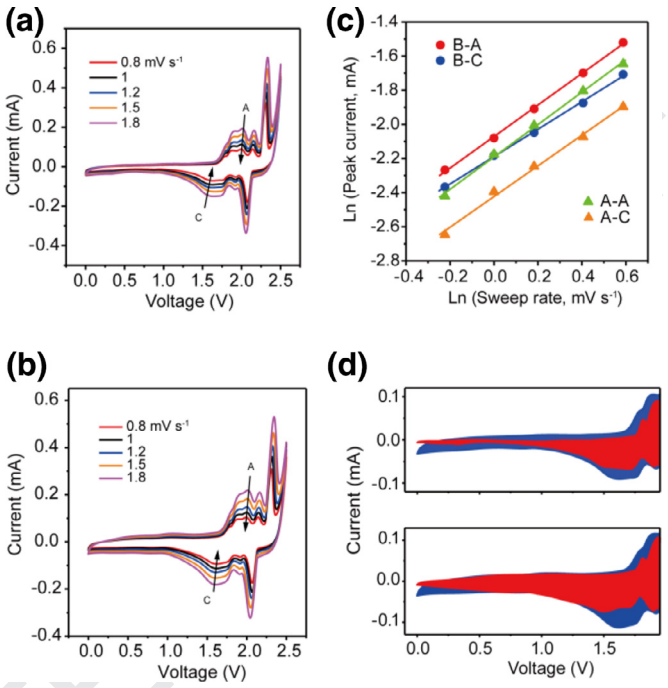


Fig. 3. CV curves of the Al-G battery at (a) a normal status with 120 mAh g^{-1} and (b) an abnormal status with 170 mAh g^{-1} in a scan range from 0.8 to 1.8 mV s^{-1}. (c) Linear relationships between ln (peak currents) and ln (sweep rates) of a anodic peak at 2.0 V and a cathodic peak at 1.6 V indicated in (a) and (b). The anodic peak A in (a) is indicated as A-A, the cathodic peak C in (a) is A-C and so on. And the sloping of B-A is 0.9236, of B-C is 0.8024, of A-A is 0.9483 and of A-C is 0.8992. (d) Capacitive (red) and diffusion-controlled (navy) contribution to charge storage in a voltage region of 0–1.95 V of 1.0 mV s^{-1} curve at (a) A and (b) B status. The contribution ratio of red region is 63.5% (top) at A status and increases to 76.7% (bottom) at B status.

110 mAh g^{-1} within 15,000 cycles as EMIC/$AlCl_3$ (r_{AlCl3}=1.5, Emi-1.5) electrolyte was used (Fig. 1b). Both of them had a stable CE over 97%. This unusual phenomenon also similarly occurred when inert Ta foil was used as the current collector (Fig. S1). These help to exclude the effect from the anodic corrosion of the current collector since Ta is much weakly corroded in those electrolytes and the corrosion cannot maintain a high CE as well [23].

Notably, the discharging/charging voltage plateaus kept stable with cycles (Fig. 1c,d). The CV plots show their corresponding cathodic/anodic peak positions stay same at the capacity of 120 and 170 mAh g^{-1} (Fig. 2a). These indicate that the dominant intercalation/de-intercalation reactions are not significantly affected. But galvanostatic voltage-capacity plots present the sloping region below 1.7 V become much flatter and have a larger sloping capacity with cycles (Fig. 1c,d). The area of CV region below the well-defined cathodic (2.0 V) and anodic (2.2 V) peak of the abnormal status with 170 mAh g^{-1} is obviously larger than that of the normal status with 120 mAh g^{-1} (Fig. 2b), suggesting a new reaction mechanism below the voltage plateaus. We further measured capacitive and diffusive-controlled effects in this CV region and the extent of the capacitive effect by plotting linear relationship between ln(scan rates) and ln(peak currents) [24,25]. The sloping of the anodic peak (2.0 V) and cathodic peak (1.6 V) at both normal and abnormal status is close to 1, indicating surface-controlled pseudocapacitive behavior for the two peaks (Fig. 3a,c) [26]. Moreover, the contribution ratio shows the capacitive current accounts at 63.5% for the common status while raising to 76.7% for the status with an ultrahigh capacity of 170 mAh g^{-1} (Fig. 3d), proving the increase proportion of adsorption-controlled capacitive behavior. As a result, the new reaction is related to capacitive-controlled behavior.

In general, the growing tendency of cathode capacity in battery and the resultant ultrahigh capacity are supposed to be induced by electrolyte or cathode, since both of two may have some changes by cycles. The electrolytic change was usually brought by self-oxidation, hydrolyzation and metallic corrosion, while the structural change of cathode can be created by the intercalation process [27,28]. By re-assembled cells with cycled electrolyte and cathode, influences from these two parts can be easily separated and investigated. The capacity performance made by the re-assembled strategies illustrates the unusually high capacity of roughly 140 mAh g^{-1} cannot be well maintained without the cycled graphene cathode. As the fresh electrolyte was substituted to the cycled electrolyte in one Al-G battery which had exhibited a high capacity of 138 mAh g^{-1}, the re-assembled battery saw a slightly declined capacity to 130 mAh g^{-1} (Fig. 4a). In contrast, as the cycled GF cathode in an Al-G battery with 142 mAh g^{-1} was replaced by a new GF, there was a remarkable drop of capacity to 90 mAh g^{-1} which is very close to an initial level of this battery prototype (Fig. 4b). Clearly, the structural change of graphene cathode by cycles is the predominant cause to stimulate a growing capacity and to a high level.

Further, a new method was developed to evaluate the increased amount of adsorption-based capacitive behavior [29–31]. We compared the capacitance of a cycled GF with a capacity of 160 mAh g^{-1} in Et-1.5 electrolyte (named CGF-Et), a cycled GF with 105 mAh g^{-1} in Emi-1.3 (CGF-Emi), and a fresh GF without any cycling (GF). These electrodes were assembled into supercapacitors by pairing each of them with a fresh GF and using $EMIBF_4$ ionic liquid as electrolyte. The specific capacitance (*Cs*) is calculated on the basis of each galvanostatic charge-discharge curve (calculation details in *Supplementary materials*). The resulting *Cs* for CGF-Et is 57.5 F g^{-1} almost twice of 33.7 F g^{-1} for the fresh GF. According to $Cs=\varepsilon_r\varepsilon_0 A/dm$ where ε_r is the relative dielectric constant of the electrolyte, ε_0 is the permittivity of vacuum, *A* is the surface area of the electrode, *m* is the mass of active materials, and *d* is charge separation distance [30,32], *Cs* almost linearly reflects the scale of *A* of the electrodes with close mass and in same electrolyte. So this indicates that CGF-Et is characterized by a larger surface area accessible to the electrolyte ions than the fresh GF (Fig. 4c,d). In addition, the Warburg region, a straight line, in Nyquist plots emerges changing sloping for the battery with a growing capacity, and the appearing region at the medium frequency (1.2 kHz–25 Hz) is ascribed to the changed interface parameters such as the porous structure (Fig. S2) [33]. We also observed graphene flakes adhering to the glass fiber separator in SEM images and an increased *D* peak for the cycled GF cathodes by Raman spectroscopy (Fig. S3). Moreover, TEM images show that the cycled GF sheets have the fewer stacked graphene layers (15–20) than that of the pristine GF

UNCORRECTED

Please cite this article as: H. Xu, H. Chen and H. Lai et al., Capacitive charge storage enables an ultrahigh cathode capacity in aluminum-graphene battery, Journal of Energy Chemistry, https://doi.org/10.1016/j.jechem.2019.09.025

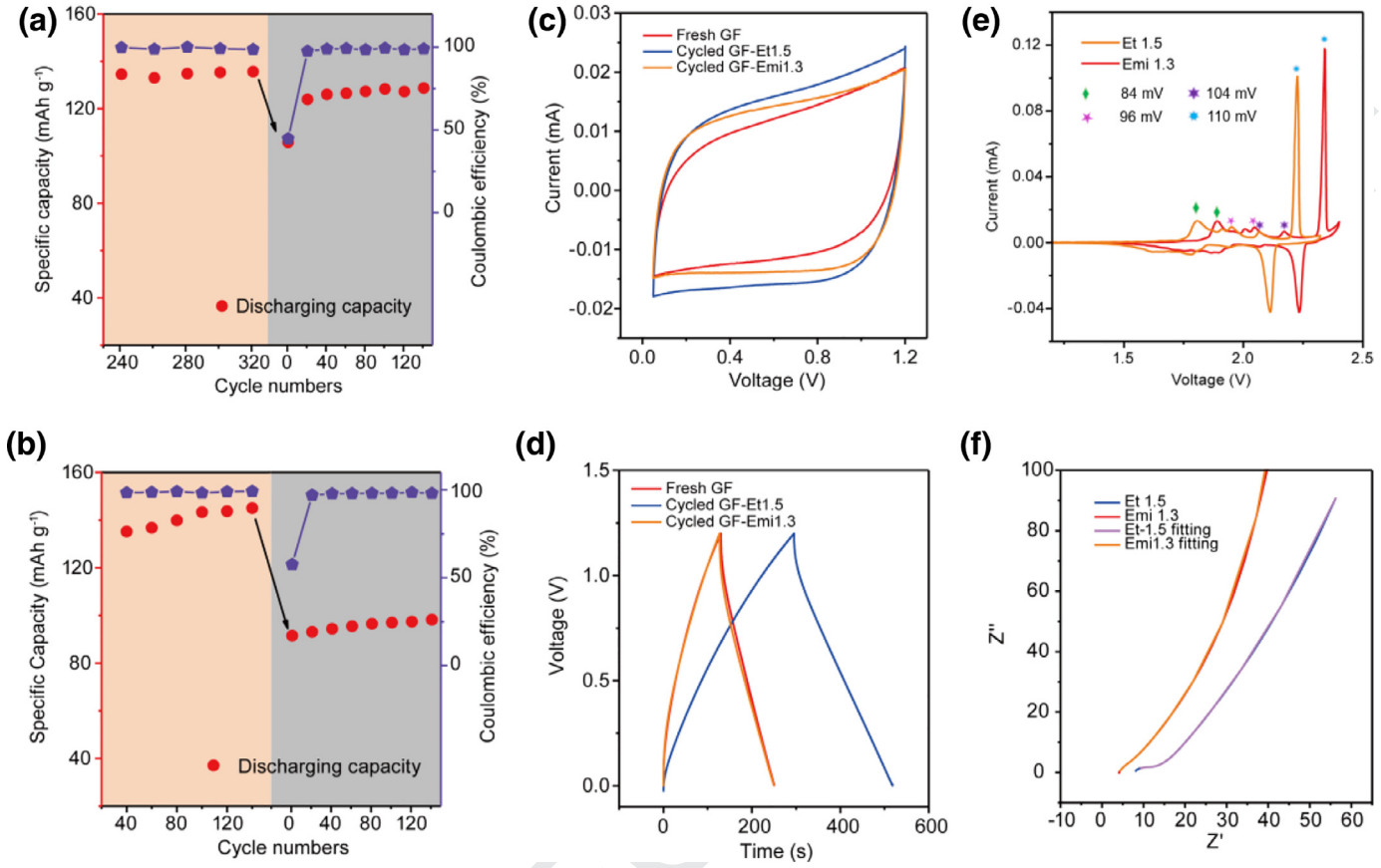


Fig. 4. In picture (a) and (b), the orange part indicates an ultrahigh discharging capacity of roughly 140 mAh g^{-1} of the Al-G batteries, and the grey part presents a change of the discharging capacity after the re-assembled strategies were implemented on the batteries. The tested Al-G batteries were assembled with Ta, GF cathode and Et-1.5 and performed at a current density of 2.5 A g^{-1}. The re-assembled strategies are (a) fresh electrolyte paired with the cycled cathode, and (b) new cathode matched with the cycled electrolyte. (c) CV curves of three capacitors using GF, CGF-Et, CGF-Emi as working electrodes paired with GF as counter electrode at a scan rate of 2 mV s^{-1}, and (d) their galvanostatic charge-discharge curves. (e) CV curves at a scan rate of 0.05 mV s^{-1}, and (f) Nyquist plots of the Al-G batteries using Emi-1.3 and Et-1.5 electrolyte after 50 cycles activation. The fitting curves are displayed using the equivalent circuits shown in Fig. S5.

and an expanded interlayer spacing to 0.38 nm (Fig. S4). These evidences point out that GF cathode is gradually exfoliated by cycling so that having more surficial vacancies for capacitive charge storage [34].

In comparison, the *Cs* for CGF-Emi is only 30.5 F g^{-1}, close to that of a fresh GF (Fig. 4c,d). This means that the structure of GF is barely changed during cycling in Emi-1.3, and CGF-Et has larger space for capacitive charge storage than CGF-Emi even though they experienced same cycles. So the graphitic cathodes cycling in Et-1.5 can be endowed with a higher contribution of capacitive storage, which helps to understand the previous reports that expanded graphite and graphene aerogel cathodes can have higher capacities as using Et-1.5 than Emi-1.3 [19,20]. Previous work has demonstrated the intercalation of $AlCl_4^-$ anions into graphene layers occurring during charging, while a reversible reaction takes place during discharging in those two electrolytes [2,19]. However, CV plots at a low scan rate of 0.05 mV s^{-1} shows the potential hysteresis between the intercalation and deintercalation of $AlCl_4^-$ for Emi 1.3 is of 10 mV larger than that of Et 1.5 (Fig. 4e). Nyquist plots also present that the charge transfer resistance (R_{ct}) is 3 times larger for Et-1.5 than Emi-1.3 (Fig. 4f, Table S1), revealing interfacial charge transfer for Et-1.5 associated with larger impedance and higher activation energy [35]. These evidences signify that the graphene sheets suffer much heavier stress/strain by the insertion process occurring in Et-1.5 [36–38]. More importantly, a stage 4 graphite intercalation compound (GIC) forming at a fully charged status with a specific capacity of 100 mAh g^{-1} in these two electrolytes can be confirmed by in situ XRD and Raman spectra (Fig. 5a,b) [39]. There are a dominant (005) peak at 22.92° ($d \approx 3.88$ Å) and a (006) peak at 27.76° ($d \approx 3.21$ Å) for GF in Et-1.5, while (005) peak at 23.40° ($d \approx 3.80$ Å) and (006) peak at 28.24° ($d \approx 3.16$ Å) for GF in Emi-1.3 (Fig. 5a, Fig. S6) [2,22]. The intercalant gallery height (d_i) is calculated of 6.0 Å for a fully charged GF in Et-1.5, larger than the counterpart of 5.7 Å in Emi-1.3; thereby it's the larger intercalants in Et-1.5 that make GF subjected to a heavier volume change during the intercalation process and cause serious exfoliation. Obviously, the different size of the intercalants in Et-1.5 and Emi-1.3 indicates that there should have other electrolyte ions intercalated except our believed $AlCl_4^-$ anions during charging.

CV plots at a low scan rate of 0.05 mV s^{-1} have shown the well-defined anodic peak at 2.23 V and 2.34 V, and other three anodic peaks at 1.8–2.2 V for both Et-1.5 and Emi-1.3 electrolyte (Fig. 4e). The potential differences of these 4 peaks are 110, 104, 96 and 84 mV, respectively. The anodic/cathodic reaction during charging is described as

$$3AlCl_4^- + 3C_n \rightarrow 3C_n^+AlCl_4^- + 3e^- \quad (2)$$

$$4Al_2Cl_7^- + 3e^- \rightarrow 7AlCl_4^- + Al \quad (3)$$

with the equilibrium electrode potential for GIC formation (E^a_{GIC}) and Al deposition (E^a_{Al}) written as

$$E^a_{GIC} = E^0_{GIC} - \frac{RT}{3F}\ln\frac{1}{a\left(AlCl_4^-\right)^3} \quad (4)$$

Please cite this article as: H. Xu, H. Chen and H. Lai et al., Capacitive charge storage enables an ultrahigh cathode capacity in aluminum-graphene battery, Journal of Energy Chemistry, https://doi.org/10.1016/j.jechem.2019.09.025

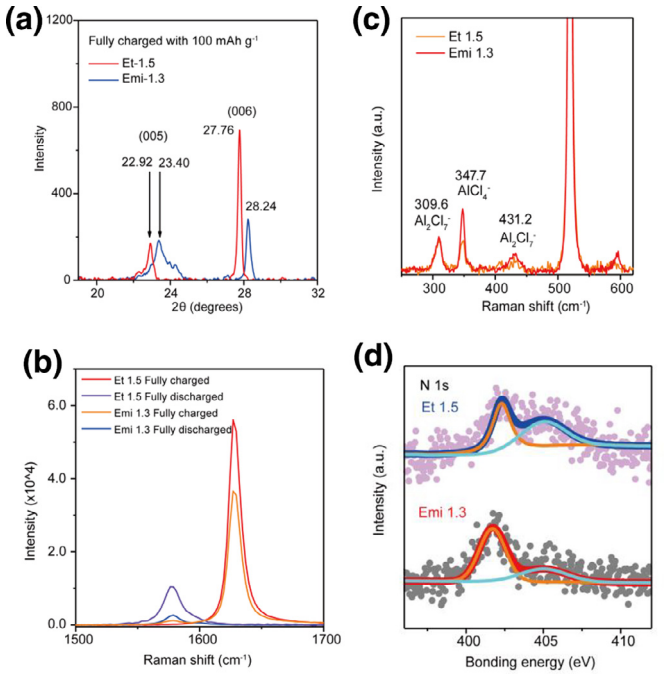


Fig. 5. (a) *In-situ* XRD spectra of GF at a fully charged status with a specific capacity of 100 mAh g^{-1}, and (b) *In-situ* Raman spectra of GF at a fully charged/discharged status in Et-1.5 and Emi-1.3 electrolyte. (c) Raman spectra of Et-1.5 and Emi-1.3 electrolyte. The signal at 520 cm^{-1} is from substrate of SiO_2, and all Raman spectra are normalized to this silicon reference. (d) XPS analysis (N 1 s) of the cycled GFs in the two electrolytes. The scattering is from original data and peak-fit results are shown in different color lines. The signal at 405 eV corresponds to N–O bond.

$$E^{a}_{Al} = E^{0}_{Al} - \frac{RT}{3F}\ln\frac{a\left(AlCl_4^-\right)^7}{a\left(Al_2Cl_7^-\right)^4} \quad (5)$$

where $\boldsymbol{E^{a}_{GIC}}$ and E^{a}_{Al} are the standard electrode potential for Eqs. (2) and (3). By Eq. (4), $\boldsymbol{E^{a}_{GIC}}$ is only affected by the activity of $AlCl_4^-$ [40,41]. We compared the ionic concentration of $AlCl_4^-$ and $Al_2Cl_7^-$ in the two electrolytes by their Raman intensities [42]. There is a half concentration of $AlCl_4^-$clusters in Et-1.5 than Emi-1.3 yet an almost same concentration of $Al_2Cl_7^-$ in the two electrolytes (Fig. 5c). Then, we estimated the difference of intercalation voltage relative to the Al anode potential (ΔE_{GIC}) in the two electrolytes according to Eqs. (4) and (5) as follows (detailed calculations in *Supplementary Information*).

$$\Delta E^{a}_{Al}(\text{Emi}-\text{Et}) = 7*\frac{RT}{3F}*\ln 2 = -42\ \text{mV} \quad (6)$$

$$\Delta E^{a}_{GIC}(\text{Emi}-\text{Et}) = \frac{RT}{F}*ln2 = 150\ \text{mV} \quad (7)$$

$$\Delta E_{GIC}(\text{Emi}-\text{Et}) = 108\ \text{mV} \approx 110\ \text{mV} \quad (8)$$

The resulting ΔE_{GIC} is 108 mV where the temperature is 298.15 K, which is very similar to 110 mV, that is, the potential difference of the dominant anodic peak (at 2.2–2.3 V) in the two electrolytes. So the voltage of this anodic peak is only associated with the activity of $AlCl_4^-$ in both Emi-1.3 and Et-1.5 and the corresponding intercalation behavior should only involve with $AlCl_4^-$ anions. However, ΔE_{GIC} for those peaks below 2.2 V is smaller than 110 mV at all (Fig. 4e). This reveals the voltages for those peaks corresponding to the onset intercalation and the low-stage GIC formation are not just related with the activity of $AlCl_4^-$. So it is at 1.8–2.2 V where have other ions intercalated. Since the intercalants at larger size in Et-1.5 than Emi-1.3 should demand higher activation energy to intercalate, it is justified that ΔE_{GIC} for the real intercalants is smaller than the value only concerned with $AlCl_4^-$ (108 mV).

Given the components in the two electrolytes, $Al_2Cl_7^-$ and cations are considered as the possible co-intercalation ions with $AlCl_4^-$. However, the galvanostatic cycling of the battery with Emi-1.5 in Fig. 1(b) does not show a constant increase of cathode capacity same as that of the battery with Et-1.5 in Fig. 1(a). This helps exclude $Al_2Cl_7^-$ and the co-intercalation of cations is suggested as a result. XPS analysis displaying N 1 *s* signals at 402 eV (405 eV for N–O bonding) for the cycled GF in the two electrolytes endorses our speculation preliminarily (Fig. 5d, S7) [43,44]. Moreover, a simple simulation also shows that the size of Et_3NH^+ is a bit larger than that of EMI^+ (Fig. S8), exactly matching our results. Certainly, our investigation will further elucidate this phenomenon and its effects on the structure of graphene cathode with more intuitive and visual evidences.

In summary, we propose a fundamental understanding of the abnormal growing trend of the cathode capacity in Al-G battery. We demonstrated that the graphene cathode is gradually exfoliated during the periodic intercalation process, which generates more surficial vacancies to enable larger capacitive charge storage and thereby, a growing cathode capacity during cycling. Precisely because of the larger intercalants in size and the resultant heavier stress on the graphene layers during the intercalation process in Et-1.5, there was the more serious exfoliation of cathode in Et-1.5 than Emi-1.3 electrolyte. The co-intercalation of cations with $AlCl_4^-$ was therefore suggested at the low intercalation voltage. The co-intercalation mechanism and the concomitant exfoliation effect enable the Al-G battery an ultrahigh cathode capacity over 150 mAh g^{-1} yet barely compromise cycle life and voltage plateaus. This new proposed principle can lead the design of the future advanced high-capacity cathode, showing great promise for developing a higher-energy-density Al-ion battery.

Declaration of Competing Interest

The authors declare no competing financial interest.

Acknowledgments

This work is supported by the National Natural Science Foundation of China (No. 51533008), National Key R&D Program of China (No. 2016YFA0200200), Key Research and Development Plan of Zhejiang Province (2018C01049), and Fujian Provincial Science and Technology Major Projects (No. 2018HZ0001-2)

Supplementary materials

Supplementary material associated with this article can be found, in the online version, at doi:10.1016/j.jechem.2019.09.025.

References

[1] H. Yang, H. Li, J. Li, Z. Sun, K. He, H.M. Cheng, F. Li, Angew. Chem. Int. Ed. 57 (2018) 1898.
[2] M.C. Lin, M. Gong, B. Lu, Y. Wu, D.Y. Wang, M. Guan, M. Angell, C. Chen, J. Yang, B.J. Hwang, H. Dai, Nature 520 (7547) (2015) 325–328.
[3] Y. Zhang, S. Liu, Y. Ji, J. Ma, H. Yu, Adv. Mater. 30 (38) (2018) 1706310.
[4] F. Wu, H. Yang, Y. Bai, C. Wu , Adv. Mater. (2019) 1806510.
[5] S.C. Jung, Y.J. Kang, D.J. Yoo, J.W. Choi, Y.K. Han, J. Phys. Chem. C 120 (25) (2016) 13384–13389.
[6] X. Yu, B. Wang, D. Gong, Z. Xu, B. Lu, Adv. Mater. 29 (4) (2017) 1604118.
[7] H. Chen, H. Xu, S. Wang, T. Huang, J. Xi, S. Cai, F. Guo, Z. Xu, W. Gao, C. Gao, Sci. Adv. 3 (12) (2017) eaao7233.
[8] H. Chen, F. Guo, Y. Liu, T. Huang, B. Zheng, N. Ananth, Z. Xu, W. Gao, C. Gao, Adv. Mater. 29 (12) (2017) 1605958.
[9] L. Zhang, L. Chen, H. Luo, X. Zhou, Z. Liu, Adv. Energy. Mater. 7 (15) (2017) 1700034.

UNCORRECTED PROOF

[10] H. Chen, C. Chen, Y. Liu, X. Zhao, N. Ananth, B. Zheng, L. Peng, T. Huang, W. Gao, C. Gao, Adv. Energy. Mater. 7 (17) (2017) 1700051.
[11] I. Hadjipaschalis, A. Poullikkas, V. Efthimiou, Renew. Sust. Energy Rev. 13 (6) (2009) 1513–1522.
[12] D. Deng, Energy Sci. Eng. 3 (5) (2015) 385–418.
[13] N. Nitta, F. Wu, J.T. Lee, G. Yushin, Mater. Today 18 (5) (2015) 252–264.
[14] C. Wu, S. Gu, Q. Zhang, Y. Bai, M. Li, Y. Yuan, H. Wang, X. Liu, Y. Yuan, N. Zhu, Nat. Commun. 10 (1) (2019) 73.
[15] Y. Hu, B. Luo, D. Ye, X. Zhu, M. Lyu, L. Wang, Adv. Mater. 29 (48) (2017) 1606132.
[16] Y. Hu, D. Ye, B. Luo, H. Hu, X. Zhu, S. Wang, L. Li, S. Peng, L. Wang, Adv. Mater. 30 (2) (2018) 1703824.
[17] Y. Wu, M. Gong, M.C. Lin, C. Yuan, M. Angell, L. Huang, D.Y. Wang, X. Zhang, J. Yang, B.J. Hwang, H. Dai, Adv. Mater. 28 (41) (2016) 9218–9222.
[18] Z. Li, Z. Xu, Y. Liu, R. Wang, C. Gao, Nat. Commun. 7 (2016) 13684.
[19] H. Xu, T. Bai, H. Chen, F. Guo, J. Xi, T. Huang, S. Cai, X. Chu, J. Ling, W. Gao, Energy Storage Mater. 17 (2019) 38–45.
[20] X. Dong, H. Xu, H. Chen, L. Wang, J. Wang, W. Fang, C. Chen, M. Salman, Z. Xu, C. Gao, Carbon 148 (2019) 134–140.
[21] G. Schmuelling, T. Placke, R. Kloepsch, O. Fromm, H.W. Meyer, S. Passerini, M. Winter, J. Power Sources 239 (2013) 563–571.
[22] S.M. Tabakman, Z. Chen, H.S. Casalongue, H. Wang, H. Dai, Small 7 (4) (2011) 499–505.
[23] S. Wang, Z. Yu, J. Tu, J. Wang, D. Tian, Y. Liu, S. Jiao, Adv. Energy Mater. 6 (13) (2016) 1600137.
[24] K. Zhao, F. Liu, C. Niu, W. Xu, Y. Dong, L. Zhang, S. Xie, M. Yan, Q. Wei, D. Zhao, L. Mai, Adv. Sci. 2 (12) (2015) 1500154.
[25] H.G. Jung, J. Hassoun, J.B. Park, Y.K. Sun, B. Scrosati, Nat. Chem. 4 (7) (2012) 579.
[26] P. Simon, Y. Gogotsi, B. Dunn, Science 343 (6176) (2014) 1210–1211.
[27] J. Liu, C.K. Poh, D. Zhan, L. Lai, S.H. Lim, L. Wang, X. Liu, N. Gopal Sahoo, C. Li, Z. Shen, J. Lin, Nano Energy 2 (3) (2013) 377–386.
[28] V. Nicolosi, M. Chhowalla, M.G. Kanatzidis, M.S. Strano, J.N. Coleman, Science 340 (6139) (2013) 1226419.
[29] X. Yang, C. Cheng, Y. Wang, L. Qiu, D. Li, Science 341 (6145) (2013) 534–537.
[30] G. Xiong, C. Meng, R.G. Reifenberger, P.P. Irazoqui, T.S. Fisher, Electroanalysis 26 (1) (2014) 30–51.
[31] Q. Yang, Z. Xu, C. Gao, J. Energy Chem. 27 (1) (2018) 6–11.
[32] P. Simon, Y. Gogotsi, Nat. Mater. 7 (2018) 845.
[33] M.D. Levi, D. Aurbach, J. Phys. Chem. B 101 (23) (1997) 4641–4647.
[34] S. Bhattacharya, A.R. Riahi, A.T. Alpas, J. Power Sources 196 (20) (2011) 8719–8727.
[35] J. Zhao, X. Zou, Y. Zhu, Y. Xu, C. Wang, Adv. Funct. Mater. 26 (44) (2016) 8103–8110.
[36] H. Kim, J. Hong, G. Yoon, H. Kim, K.Y. Park, M.S. Park, W.S. Yoon, K. Kang, Energy Environ. Sci. 8 (10) (2015) 2963–2969.
[37] D. Kundu, S. Hosseini Vajargah, L. Wan, B. Adams, D. Prendergast, L.F. Nazar, Energy Environ. Sci. 11 (4) (2018) 881–892.
[38] C.J. Pan, Y. Rong, C. Yuan, M.C. Lin, B.J. Hwang, H. Dai, Proc. Natl. Acad. Sci. USA 114 (5) (2017) 834.
[39] H. Moon, R. Tatara, T. Mandai, K. Ueno, K. Yoshida, N. Tachikawa, T. Yasuda, K. Dokko, M. Watanabe, J. Phys. Chem. C 118 (35) (2014) 20246–20256.
[40] X. Wu, Y. Xu, C. Zhang, D.P. Leonard, A. Markir, J. Lu, X. Ji, J. Am. Chem. Soc. 141 (15) (2019) 6338–6344.
[41] B. Gilbert, H. Olivier-Bourbigou, F. Favre, Oil Gas Sci. Technol. 62 (6) (2007) 745–759.
[42] K. Beltrop, P. Meister, S. Klein, A. Heckmann, M. Grünebaum, H.-.D. Wiemhöfer, M. Winter, T. Placke, Electrochim. Acta 209 (2016) 44–55.
[43] O. Höfft, S. Bahr, M. Himmerlich, S. Krischok, J.A. Schaefer, V. Kempter, Langmuir 22 (17) (2006) 7120–7123.
[44] J. Ananpattarachai, P. Kajitvichyanukul, S. Seraphin, J. Hazard. Mater. 168 (1) (2019) 253–261.

UNCORRECTED PROOF

Please cite this article as: H. Xu, H. Chen and H. Lai et al., Capacitive charge storage enables an ultrahigh cathode capacity in aluminum-graphene battery, Journal of Energy Chemistry, https://doi.org/10.1016/j.jechem.2019.09.025